

Supporting Information for Publication: Oxygen Evolution Reaction Kinetic Barriers on Nitrogen-Doped Carbon Nanotubes

Lauri Partanen, Garold Murdachaew, and Kari Laasonen*

*Department of Chemistry and Material Science, Aalto University, P.O. Box 16100,
FIN-00076 Aalto, Finland*

E-mail: kari.laasonen@aalto.fi

1 Methods for the creation of the initial and final NEB images

As described in Section 2 of the main article, the initial images for the solvated CI-NEB calculations were created by a two-step relaxation process, where first the positions of an inner layer of five water molecules for step (1) and six for step (3) were optimised, followed by a relaxation of the remaining water molecules with the positions of the inner waters fixed. In both N-doped CNTs, the OH^- group showed great mobility with a strong tendency to travel to the droplet surface and end up in a fourfold-coordinated $\text{OH}^-(\text{H}_2\text{O})_4$ state, in line with the studies on hydroxide ion mobility by Tuckerman et al.^{1,2} To solve this problem, one of the water molecules adjacent to the OH^- was fixed throughout the geometry optimisation of the initial images of step (1). A second issue pertained to the final images of the NEB calculations for step (3). In the case of N_2CNT , the $^*\text{OOH}$ desorbed from the surface when the number of relaxed water molecules was too small (e.g., when only the same six core

water molecules were optimised as during the construction of the initial image). Several solutions were attempted to tackle this issue. In the first, a droplet configuration with one OH^- was first optimised in two stages, again starting with the initial relaxation of an inner core of 5-6 waters, parts of the CNT near the active site, and the OH^- , followed by a separate optimisation of the remaining water molecules. The obtained droplet structure was then utilised for *each* of the initial images of the different reaction steps. Depending on the location of the active site and surface adsorbates present, the whole droplet could be slightly raised or shifted along the surface. Thus, in this approach, the number of water molecules within the droplet stayed the same throughout. However, this was also an issue as it was challenging to fit surface adducts like $^*\text{OH}$ and $^*\text{OOH}$ into the centre of the water droplet without artificially raising the droplet significantly higher from the tube surface. We also encountered severe issues with the stability of the final image, so in the end, this scheme was dropped.

In the second attempted scheme, at first, full optimisation of all water molecules and the two nearest neighbour carbon or nitrogen atoms to the active site was conducted for the *final* image. As was the case in the adopted NEB methodology, the reacting OH^- was created by subtracting a hydrogen atom from one of the water molecules near the active site. Once the final image was relaxed, the initial image was formed by taking the $^*\text{OH}$ from the reaction site and moving it to the place of its originating water molecule, followed by a reoptimisation of about 5-6 neighbouring water molecules and the OH^- . In this approach, the main problem was that the OH^- tended to return to the reaction site, reforming the final image during the geometry optimisation. This coupled with additional issues of the OH^- diffusing to the surface of the droplet if the number of active water molecules in the initial image geometry optimisation was increased led us to abandon this scheme as well.

In the third scheme, we simply increased the number of optimised water molecules for the final image. After carefully testing how many waters should remain active, we settled on 18, as this way the majority of H_2O molecules remained fixed throughout the NEB calculation.

On the other hand, this number was large enough so that the C–O bond was not very strained compared to the fully relaxed value (1.60 versus 1.58 Å) and yet sufficiently small to prevent substantial changes in droplet geometry. In contrast, if a full optimisation of the droplet was carried out, a restructuring of geometry occurred resulting in a slightly lower average hydrogen bond length and a lowering of the system energy by some tenths of an eV, in addition to possible changes in the potential arising from this restructuring during the NEB calculation.

2 The effect of convergence criteria on the NEBs

We performed several test calculations on the impact of NEB convergence criteria on the shape of the NEB. All the bare and solvated NEB calculations presented in the article were done with the convergence criterion for the maximum force component of the configuration first set to 0.21 eV/Å. For the solvated NEB calculations, this was tightened to 0.10 eV/Å. In comparing the resulting NEBs, we observed no significant changes in the predicted minimum energy paths, and the barrier heights between the calculations employing different convergence criteria were within 0.05 eV/Å in all cases. Because the third OH⁻ attachment reaction (step (3)) for the solvated N₂CNT OER was one of the hardest to converge, we used it to explore the effect of convergence further. This was done by setting the maximum force convergence criterion to its default value of 0.023 eV/Å with corresponding decreases in other three convergence criteria employed by CP2K (maximum band displacement, root-mean-square displacements of the band, and root-mean-square force). The resulting three NEB curves are shown in Figure S1, where one can see that the differences between the NEB obtained with the tighter convergence criteria does not differ from the other two in any meaningful way. The results of our solvated CNT NEB calculations indicate that at last in systems similar to the one studied here, one can substantially loosen the NEB convergence criteria without a significant loss to the accuracy of the results.

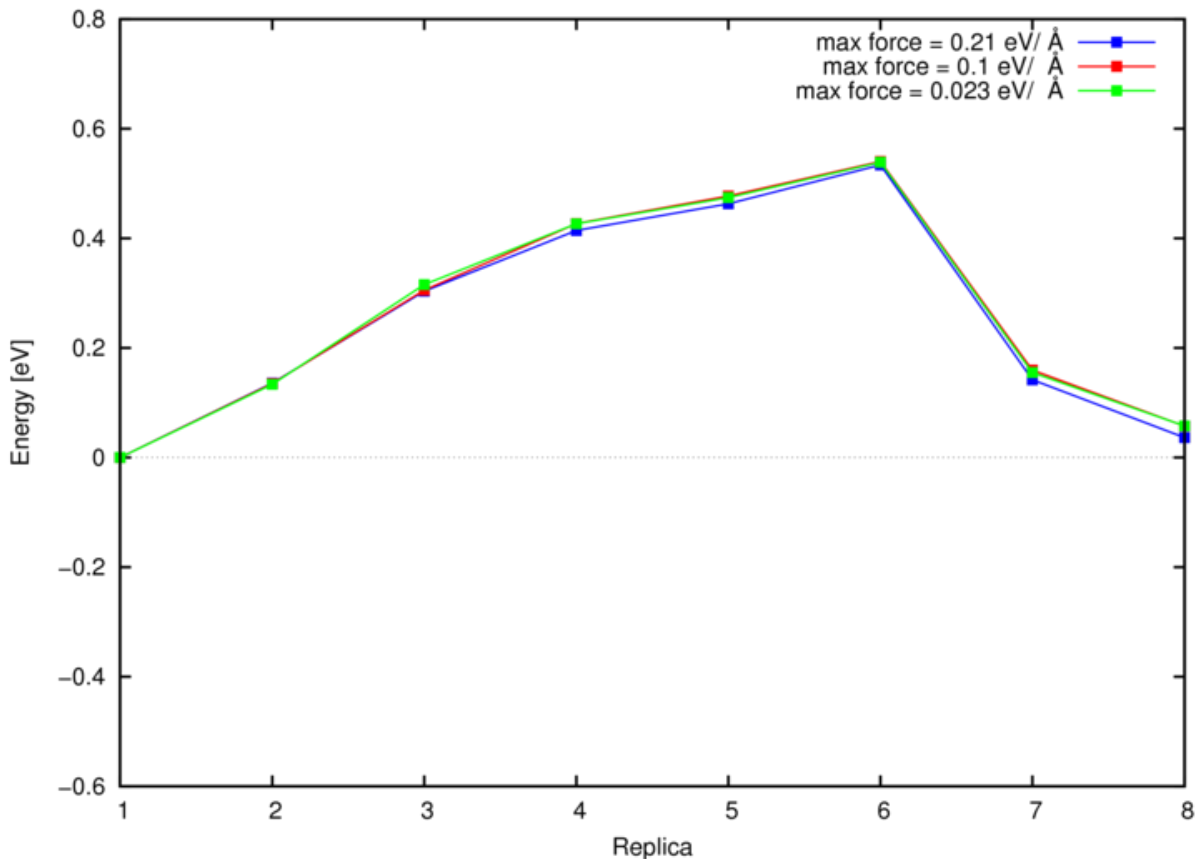


Figure S1: Convergence test for the *OOH formation step (step (3)) for N₂CNT with solvent.

3 Additional NEB calculations

In addition to the NEB calculations reported in the main article, we performed a series of NEB calculations to test the impact of various DFT and NEB calculation parameters on the reaction barriers. We also tested some alternative OER reaction pathways such as a ROC-type mechanism,³ but these all proved substantially higher in energy than the reported processes. The impact of the changing positions of the linearly interpolated water molecules to the reaction barrier was also investigated by limiting the number of geometry optimised water molecules from 18 down to five for the final image of the first reaction step. This resulted in an increase in the barrier height of less than 0.1 eV, which is still within the acceptable limits.

As a point of interest, we also studied the reaction barrier at a site corresponding to site

3 in a singly doped carbon nanotube, (see Figure 1 panel D of the article). In this case, the reaction barrier was lowered to around 0.2 eV from the N₂CNT value of 0.5 eV. Still, it is larger than the site 2 value for the NCNT. Our preliminary calculations also included solvated test NEBs for site 1 in the studied pristine, NCNT and N₂CNT systems. The chief difference in these calculations to the ones presented in the article proper was that a full geometry-optimisation was carried out also for the final image, implying that all the water molecules were moving during the NEB due to linear interpolation. In these calculations, step (3) was also found to be the rate-limiting one, with reaction barriers in the range 0.5–0.9 eV.

4 Tube extension calculations

We investigated the effect of extending the tube on the solvated N₂CNT and NCNT by taking the initial, transition, and final states of the NEB where the maximum force component convergence criterion had been set to 0.21 eV/Å and increasing the length of the tube from 6 units of (14,0) CNT first to 7 and then to 8 units. This was done to ensure that the droplet images did not interact with each other, that the NEB energies were properly converged, and that the lack of *k*-points in our calculations did not give rise to any computational issues. The results are summarised in Figure S2 for steps (1) and (3). The figure demonstrates that extending the tube has a minimal effect on the calculated energies.

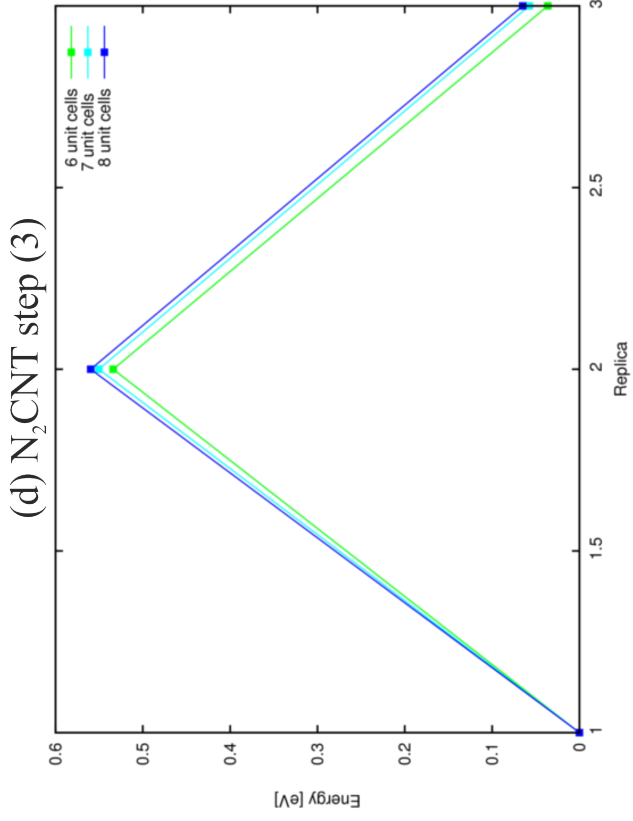
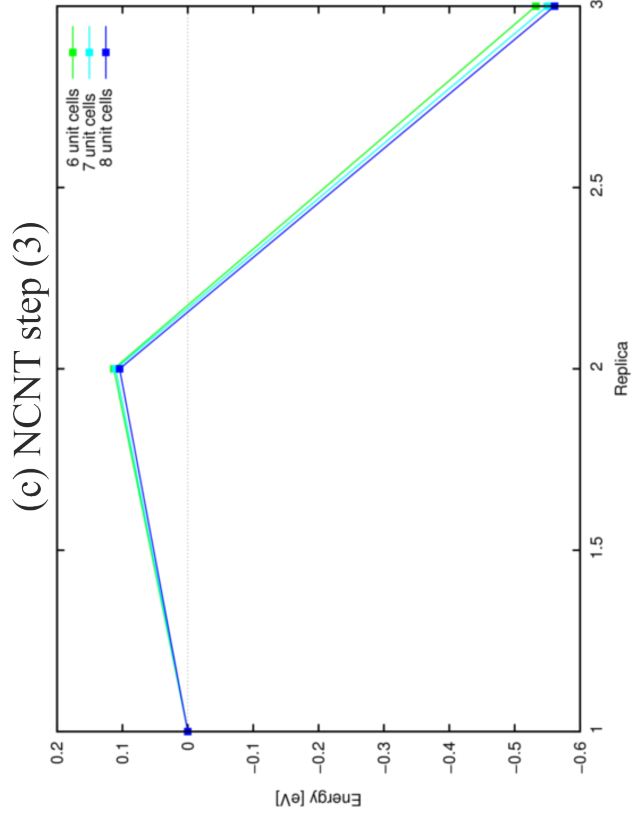
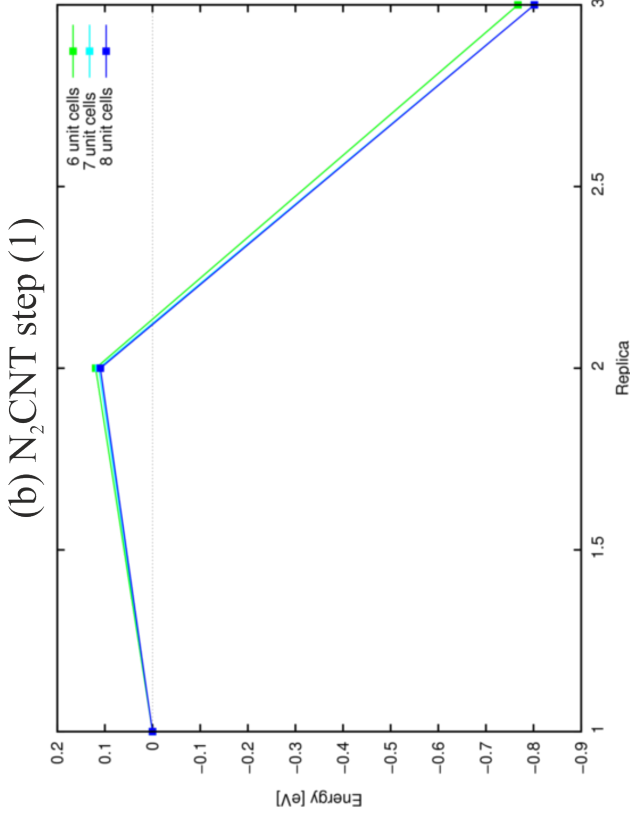
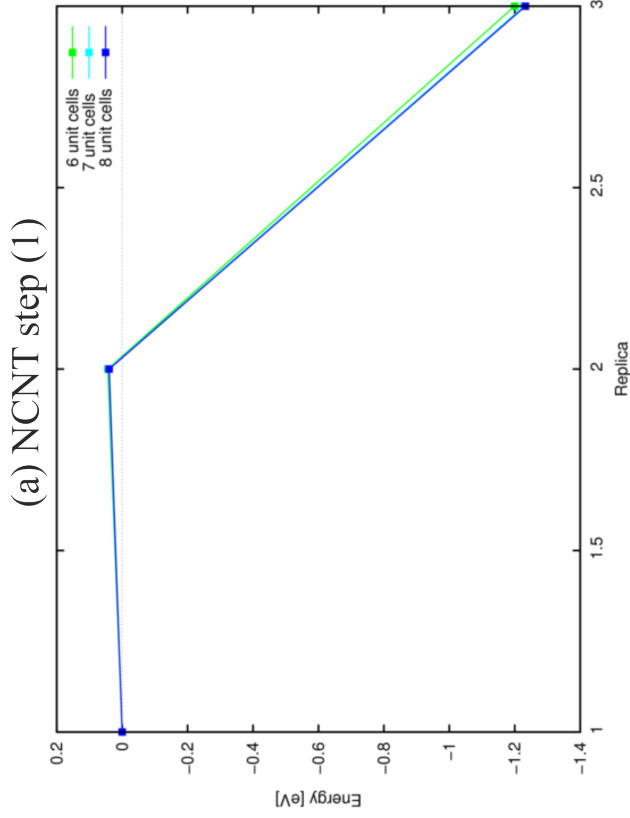


Figure S2: The effect of tube extension on the relative initial, transition state and final state energies for OER steps (1) and (3).

5 Summary of key energetic and geometrical parameters of the solvent-free and solvated NEB calculations

Table S1: Energies of the initial state (IS), transition state (TS), and final state (FS) relative to the initial state in eV.

NCNT	Solvent-free CNT			Solvated CNT		
	IS	TS	FS	IS	TS	FS
1st OER step (*OH)	0.0		-2.26	0.0	0.04	-1.20
3rd OER step (*OOH)	0.0	0.09	-1.63	0.0	0.12	-0.52
N ₂ CNT	Solvent-free CNT			Solvated CNT		
	IS	TS	FS	IS	TS	FS
1st OER step (*OH)	0.0		-1.72	0.0	0.07	-0.76
3rd OER step (*OOH)	0.0	0.12	-0.91	0.0	0.54	0.06
CNT	Solvent-free CNT					
	IS	TS	FS			
1st OER step (*OH)	0.0		-1.28			
3rd OER step (*OOH)	0.0	0.08	-1.29			

Table S2: Geometric parameters of the initial state (IS), transition state (TS), and final state (FS) in Å.

NCNT	Solvent-free CNT			Solvated CNT		
	IS	TS	FS	IS	TS	FS
1st OER step (*OH)						
$d_{\text{O-H}}$	0.98	-	0.98	0.98	0.97	1.01
$d_{\text{C-OH}}$	4.77	-	1.45	2.88	2.57	1.43
3rd OER step (*OOH)						
$d_{\text{OO-H}}$	0.98	0.98	0.99	0.98	0.99	1.02
$d_{\text{O-OH}}$	6.11	2.91	1.48	2.75	2.35	1.47
$d_{\text{C-OOH}}$	1.30	1.31	1.47	1.33	1.35	1.51
N ₂ CNT	Solvent-free CNT			Solvated CNT		
	IS	TS	FS	IS	TS	FS
1st OER step (*OH)						
$d_{\text{O-H}}$	0.98	-	0.97	0.98	0.97	1.01
$d_{\text{C-OH}}$	4.77	-	1.48	2.91	2.68	1.49
3rd OER step (*OOH)						
$d_{\text{OO-H}}$	0.98	0.98	0.99	0.98	0.99	1.01
$d_{\text{O-OH}}$	6.40	2.61	1.47	2.74	1.82	1.47
$d_{\text{C-OOH}}$	1.55	1.49	1.54	1.37	1.44	1.60
CNT	Solvent-free CNT					
	IS	TS	FS			
1st OER step (*OH)						
$d_{\text{O-H}}$	0.98	-	0.98			
$d_{\text{C-OH}}$	4.77	-	1.48			
3rd OER step (*OOH)						
$d_{\text{OO-H}}$	0.98	0.98	0.99			
$d_{\text{O-OH}}$	6.41	2.60	1.47			
$d_{\text{C-OOH}}$	1.48	1.46	1.54			

6 Construction of the relative energy step plot in Figure 6 of the main article

The stepped plot of Figure 6 was constructed by comparing the reaction energies of neighbouring OER steps with one another. For each step, the presence of OH^- that had not yet participated in OER was accounted for by adding the energy of that many OH^- species and removing an equal amount of water molecules so that the number of atoms in the system remained constant throughout. As in the thermodynamic model for estimating OER activity where the reference potential is set to the standard hydrogen electrode, the OH^- energy was calculated as $E_{\text{OH}^-} = E_{\text{H}_2\text{O}} - \frac{1}{2}E_{\text{H}_2}$, where $E_{\text{H}_2\text{O}}$ and E_{H_2} are the gas phase values of water and hydrogen, respectively.⁴⁻⁶ We used the values calculated by Murdachaew and Laasonen for these quantities, namely $E_{\text{H}_2} = -31.557$ eV and $E_{\text{H}_2\text{O}} = -468.191$ eV.⁷ For example, the initial energy for the $^*\text{OH}$ formation (step (1)) was obtained from

$$E_{1,i} = E_{\text{CNT}\cdot 45\text{H}_2\text{O}} + 4E_{\text{OH}^-} - 4E_{\text{H}_2\text{O}} = E_{\text{CNT}\cdot 45\text{H}_2\text{O}} - 2E_{\text{H}_2},$$

where $E_{\text{CNT}\cdot 45\text{H}_2\text{O}}$ is the energy of the droplet-nanotube system, without any OH^- 's present. The energy of the final state for step (1) was then calculated from

$$E_{1,f} = E_{(\text{CNT}+^*\text{OH})\cdot 44\text{H}_2\text{O}} + 3E_{\text{OH}^-} - 3E_{\text{H}_2\text{O}} = E_{(\text{CNT}+^*\text{OH})\cdot 44\text{H}_2\text{O}} - \frac{3}{2}E_{\text{H}_2},$$

where $E_{(\text{CNT}+^*\text{OH})\cdot 44\text{H}_2\text{O}}$ is the energy of the nanotube system with the $^*\text{OH}$ on the surface of the tube. The thermodynamic energy change in the first step was then obtained from $E_{1,f} - E_{1,i}$. The discovered reaction barrier energies were added to this value to form the bumps shown in Figure 6. For the final state of the O_2 formation in step (4), we used the energy of the CNT with 43 water molecules and the O_2 solvated within the droplet. In this state, the triplet O_2 molecule was at least 2.3 Å above the CNT surface. The O–O distance was around 1.3 Å.

7 Impact of *OH coverage and system charge

To estimate the effect of changing potential on the reaction barriers, we did a series of test calculations with various system charges ($q = \pm 1, \pm 2$; in addition to the neutral system with $q = 0$) for the solvated systems. The results for the relative energies of the initial, transition, and final states are reported in Table S3. As periodic systems cannot possess a net charge, a homogeneous background charge was utilised to counteract the effects of the added or removed electron. In all cases, the positions of the atoms on the CNT were relaxed while the rest of the system was kept fixed. This resulted in no significant changes in geometry. Because the geometries of the chargeless system were utilised throughout and no actual NEB calculations were performed to obtain the true transition state energies for the charged systems, the transition states in these cases have been placed in parenthesis. At most, these energies provide a qualitative indication of the behaviour of the kinetic barriers in the charged systems.

As expected, in all cases the removal of electrons from the CNT results in higher attraction between it and the electron-rich *OH or *OOH surface species which is seen as a lowering of the final state energy relative to the initial state one when one moves up in system charge. This implies a lowering of the steps in Figure 6 of the main article. Similarly, the thermodynamic barrier for the *OOH formation reaction (step(3)) is seen to go down for both NCNT and N₂CNT. While the barrier is negligible for *OH formation (step (1)), there is substantial variation in its value as the charge changes. This can be explained by the fact that shape of the minimum energy path is expected to change depending on the charge. As in the case of the tube extension calculations, the values reported in Table S3 were calculated from the NEB results where the maximum force component convergence criterion was set to 0.21 eV/Å, so they differ slightly for the $q = 0$ case from the values shown in Table S1 where the criterion was 0.1 eV/Å.

Finally, we also performed some test calculations to look at the effect of *OH coverage on the system energies. We observed, for example, the relative energy difference for step (1)

Table S3: Energies (eV) of the initial state (IS), transition state (TS), and final state (FS) relative to the initial state with non-zero system charge ($q = \pm 1, \pm 2$) compared to the neutral system results ($q = 0$) in the solvated calculations.

NCNT (step (1))					
q	2	1	0	-1	-2
IS	0.0	0.0	0.0	0.0	0.0
TS	(0.01)	(-0.84)	0.04	(-0.71)	(-0.58)
FS	-1.43	-1.30	-1.20	-1.04	-0.85
NCNT (step (3))					
q	2	1	0	-1	-2
IS	0.0	0.0	0.0	0.0	0.0
TS	(-0.09)	(-0.02)	0.11	(0.22)	(0.45)
FS	-1.01	-0.79	-0.53	0.27	0.83
N ₂ CNT (step (3))					
q	2	1	0	-1	-2
IS	0.0	0.0	0.0	0.0	0.0
TS	(-0.27)	(-0.08)	0.53	(0.93)	(1.16)
FS	-0.85	-0.59	0.04	0.55	0.86

on NCNT with an additional *OH attached to the third nearest neighbour from the reaction site and second nearest neighbour of the N dopant, changed the relative energy of the final state by less than 0.1 eV. To allow the water droplet to accommodate for the presence of the *OH adequately, in these calculations, all the water molecules were relaxed in the final image. In contrast, for the initial image the positions of the six inner shell water molecules were taken from the original step (1) calculations for NCNT and only the outer shell of 35 water molecules was optimised.

References

- (1) Tuckerman, M. E.; Marx, D.; Parrinello, M. The nature and transport mechanism of hydrated hydroxide ions in aqueous solution. *Nature* **2002**, *417*, 925–929.
- (2) Tuckerman, M. E.; Laasonen, K.; Sprik, M.; Parrinello, M. Ab initio molecular dynamics simulation of the solvation and transport of H_3O^+ and OH^- ions in water. *J. Phys. Chem.* **1995**, *99*, 5749–5752.
- (3) Hessels, J.; Detz, R. J.; Koper, M. T. M.; Reek, J. N. H. Rational design rules for molecular water oxidation catalysts based on scaling relationships. *Chem. Eur. J.* **2017**, *23*, 16413–16418.
- (4) Rossmeisl, J.; Logadottir, A.; Nørskov, J. K. Electrolysis of water on (oxidized) metal surfaces. *Chem. Phys.* **2005**, *319*, 178 – 184.
- (5) Man, I. C.; Su, H.-Y.; Calle-Vallejo, F.; Hansen, H. A.; Martínez, J. I.; Inoglu, N. G.; Kitchin, J.; Jaramillo, T. F.; Nørskov, J. K.; Rossmeisl, J. Universality in oxygen evolution electrocatalysis on oxide surfaces. *ChemCatChem* **2011**, *3*, 1159–1165.
- (6) Rossmeisl, J.; Qu, Z.-W.; Zhu, H.; Kroes, G.-J.; Nørskov, J. K. Electrolysis of water on oxide surfaces. *J. Electroanal. Chem.* **2007**, *607*, 83 – 89.

- (7) Murdachaew, G.; Laasonen, K. Oxygen evolution reaction on pristine and nitrogen-doped carbon nanotubes. Submitted to *ACS Catal.* **2018**, Manuscript ID: cs-2018-01211g.